Acta Oceanol. Sin., 2019, Vol. 38, No. 7, P. 107–113
https://doi.org/10.1007/s13131-019-1462-4
http://www.hyxb.org.cn
E-mail: hyxbe@263.net

Pore pressure observation: pressure response of probe penetration and tides

Tao Liu[1, 2*], Guanli Wei[1], Hailei Kou[1, 3], Lei Guo[4]

[1] Shandong Provincial Key Laboratory of Marine Environment and Geological Engineering, Ocean University of China, Qingdao 266100, China

[2] Laboratory for Marine Geology, Pilot National Laboratory for Marine Science and Technology (Qingdao), Qingdao 266061, China

[3] College of Engineering, Ocean University of China, Qingdao 266100, China

[4] Qingdao Institute of Marine Geology, China Geological Survey, Qingdao 266071, China

Received 28 September 2018; accepted 24 December 2018

Abstract

Excess pore water pressure is an important parameter that can be used to analyze certain physical characteristics of sediment. In this paper, the excess pore water pressure of subseafloor sediment and its variation with tidal movement was measured following the installation of a wharf in Qingdao, China by using a fiber Bragg grating (FBG) piezometer. The results indicated that this FBG piezometer is effective in the field. The measured variation of excess pore water pressure after installation is largely explained by the dissipation of excess pore water pressure. The dissipation rate can be used to estimate the horizontal consolidation coefficient, which ranged from 1.3×10^{-6} m^2/s to 8.1×10^{-6} m^2/s. The measured values during tidal phases are associated with the variability of tidal pressure on the seafloor and can be used to estimate the compressibility and the permeability of the sediment during tidal movement. The volume compression coefficient estimated from tidal oscillation was approximately 2.0×10^{-11} Pa^{-1}, which was consistent with the data from the laboratory test. The findings of this paper can provide useful information for *in situ* investigations of subseafloor sediment.

Key words: pore pressure, *in situ* observation, penetration, tidal load

Citation: Liu Tao, Wei Guanli, Kou Hailei, Guo Lei. 2019. Pore pressure observation: pressure response of probe penetration and tides. Acta Oceanologica Sinica, 38(7): 107–113, doi: 10.1007/s13131-019-1462-4

1 Introduction

Pore water pressure refers to the pressure of fluid in the voids (pores) between individual particles in the sedimentary layer. Pore pressure exists in both saturated and unsaturated sediments. Pore water pressure, as an important mechanical parameter of the sediment, can be used to analyze certain basic physical and mechanical parameters in the deposit (Bennett et al., 1982, 2002). The concept of effective stress is essential in understanding pore water pressure. The differential pressure, ΔU (often called "excess pore pressure" when it is greater than the hydrostatic pressure), is given by U–U_h. The effective stress largely controls the strength and deformation behavior of unconsolidated sediments. According to the principle of effective stress (Terzaghi, 1943), an increase in pore pressure will lead to a decrease in the vertical effective stress, leading to a reduction in shear strength (Baligh, 1986). With deeper submarine exploration and resource development, submarine landslide and foundation stability may be encountered under different depositional types (Ye, 2011). Marine landslides may occur in the entire sea environment, including shallow sea, near-shore to continental shelf, and deep ocean, and several seabed landslides that are harmful to seabed engineering structures have been recorded in offshore oil areas around the world (Vanneste et al., 2014). In addition, rapid deposition, gas escape or advection caused by geothermal gradients may result in excess pore pressure in sedimentary environments (Schultheiss and McPhail, 1986; Schultheiss, 1990; Urgeles et al., 2000), as instability in the foundation of the seabed structure can readily occur (Sultan et al., 2007; Liu et al., 2018). It is of vital importance for any submarine engineering project to determine the risk area through *in situ* observation of the pore pressure of the sediment, especially in deep-sea oil and gas resource extraction areas and areas with steep slopes (Sultan et al., 2009). Although seabed instability can be induced by earthquakes, storm surges and high-pressure gas-liquid ejection, it is difficult to determine the exact cause or timing of deformation damage.

Many studies have been carried out by scientists who are interested in geohazards and by engineers interested in *in situ* geotechnical properties as they apply to problems of offshore construction and gas-hydrate exploitation. The first known reported uses of a differential piezometer were by Lai et al. (1968) and Richards et al. (1975) using piezometers built at the Norwegian Geotechnical Institute (NGI) and the University of Illinois (UI). This so-called NGI-UI probe was deployed several times in 1967

Foundation item: The National Natural Science Foundation of China under contract Nos 41672272 and 41427803; the Science and Technology Development Project of Shandong, China under contract No. 2017GGX30125; the Guangzhou Marine Geological Survey Entrustment Project under contract No. 2017C-03-162.
*Corresponding author, E-mail: ltmilan@ouc.edu.cn

in the Wilkinson Basin, Gulf of Maine. Later, Sills and Nageswaran (1984) built and used a differential piezometer at Oxford University (OU). *In situ* data of the OU piezometer primarily investigated the effects of gas on the measured pressure response caused by tidal cycles. An autonomous Pop-Up Pore-Pressure Instrument (PUPPI) was constructed to accurately measure *in situ* pore pressure gradients in deep-sea sediments (McPhail and Schultheiss, 1986). Significant pore pressure gradients were measured in the Mariana Trough, a back-arc basin, indicating local upward flow of pore water. Sultan et al. (2009) deployed a series of piezometers to observe excess pore pressure in order to distinguish the sediment failures triggered by the Great Sumatra Earthquake from older sediment failures in France. Also in France, Sultan et al. (2014) used an IFREMER (French Research Institute for Exploitation of the Sea) piezometer to observe excess pore pressure and to investigate whether or not the shape and morphology of pockmarks could be controlled by gas-hydrate dynamics or seafloor instabilities and deformation processes. The complete *in situ* pore pressure recording contains three components (Schultheiss, 1990). Part one of the recording is dominated by the decay of a pressure pulse caused by probe penetration, which gradually dissipates over time due to the recovery of the plastic deformation zone (Burns and Mayne, 1998; Sultan and Lafuerza, 2013). *In situ* permeability can be estimated by the rate of decay of this pulse (Bennett and Fairs, 1979; Hurley and Schultheiss, 1990). Part two of the recording is a low-amplitude oscillation associated with tidal pressure variation on the seafloor, which conforms to the theory of hole expansion and is applied to the mechanism analysis of geotechnical testing instruments (Li, 2007). The amplitude and phase of these oscillations can be used to estimate *in situ* permeability and elastic modulus (Hurley, 1989; Hurley and Schultheiss, 1990; Burns and Mayne, 1998; Sultan and Lafuerza, 2013). Part three is residual pore pressure, which can be negative or positive. Excess pore pressure gradients provide direct evidence of advection of pore fluids in the sediment (Schultheiss and McPhail, 1986; Davis et al., 1991). Although much work has been done in the past forty years, weaknesses still exist in the reliability and completeness of the data, as well as the cost of equipment and the effectiveness of the method.

This paper presents a new piezometer based on fiber Bragg grating (FBG) technology and an analysis of the recorded measurements for estimating *in situ* permeability. We adopt and improve previous equipment and models to calculate the permeability of the marine sediment and investigate the reliability and completeness of the data. A study of the pore pressure in sedimentary basins can improve the understanding of the hydrologic circulation.

2 Piezometer based on fiber Bragg grating sensing technology

In this paper, according to the principle of differential pore pressure measurement, a set of observation rods for pore pressure observation of seabed sediments is designed to allow the long-term observation of pore pressure in the seabed sediments *in situ*; the principle of differential pore pressure measurement is shown in Fig. 1.

The observation equipment includes two main parts: the pore pressure measuring probe and the self-capacitive collection storage device. The pore pressure measuring rod penetrates into the sediment to detect the pore pressure (Liu et al., 2015). The acquisition and storage device is responsible for the control of the sensor signal and is connected to the probe by an installed fiber optic connector. The overall structure of the equipment is shown in Fig. 2. The pore pressure measuring probe utilizes a hollow stainless steel rod body, the sidewall of the probe is equipped with an environmental pressure sensing port, the inside of the port is composed of permeable stone, and the inner wall is embedded with the fiber grating pressure difference sensor and is used to measure the pore pressure (Li, 2015). The seal ring is used to create a waterproof seal on the inside of the probe of the environmental pressure sensing port so that the inner and outer pressures of the probe rod are separated. The top of the probe is connected with the sea water as a reference pressure port acting on the other end of the fiber grating differential pressure sensor. The two-way independent and open mode is adopted to realize real-time calibration of the pressure inside and outside the probe.

The FBG pressure sensor is a customized product, and the corrosion resistance of the FBG pressure sensor can increase its durability in deep water. The pressure value can be calculated using the following formula:

$$(\lambda_{B1} + \lambda_{B2}) / \lambda_{B0} = K\varepsilon\Delta\varepsilon + K_t\Delta t, \tag{1}$$

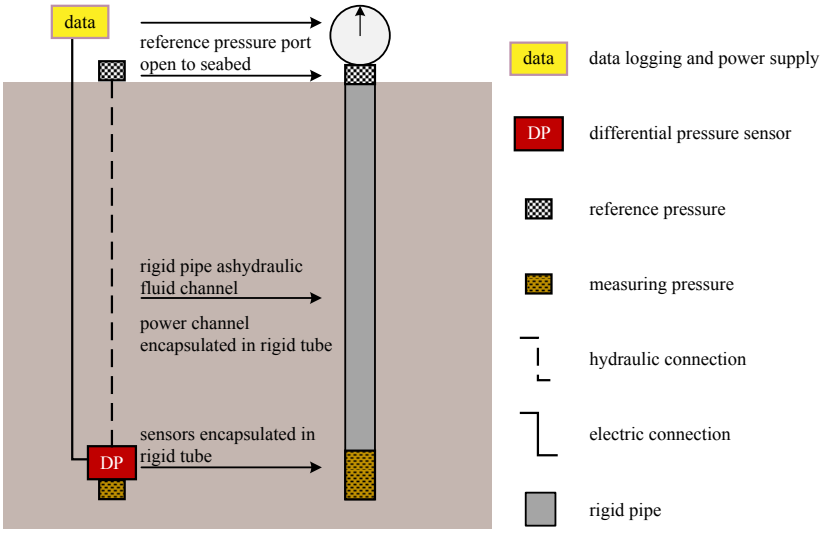

Fig. 1. The principle of differential pore pressure measurement.

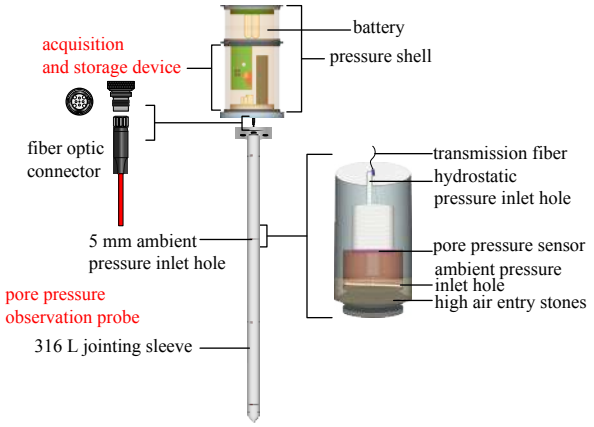

Fig. 2. The structure of the pore pressure observation probe of marine sediments.

where K_ε and K_t are the strain and temperature sensitivity coefficients, respectively; λ_{B0} is the Bragg wavelength of the grating before monitoring; λ_{B1} is the wavelength shift caused by pressure; and λ_{B2} is the wavelength shift caused by temperature.

3 *In situ* observation

3.1 *Field site*

The site of the observation is located in the Gulf of Laoshan Mountain, a port (36°20′N, 120°44′E) in Ao Shan Wei Town, Jimo, between Jiaozhou Bay and the Gulf of Ding, Shandong, China. The area has been altered as a result of local pier construction. The observation site is located in a 10-m extension of the wharf, and the surface of the seabed is composed of silt with a thickness of 3–5 m, with underlying bedrock for the construction of the wharf.

3.2 *Observation probe of pore pressure*

In long-term observations performed in December 2017, a 4.0 m-long pore pressure type I probe was used; only 0.5 m was added at the end of the probe, while the rest of the structure remained unchanged. The two observation rods were separately recorded as “pore pressure probe rod 1” and “pore pressure probe rod 2”. The sensor numbers and relative positions of the probe rods are shown in Fig. 3.

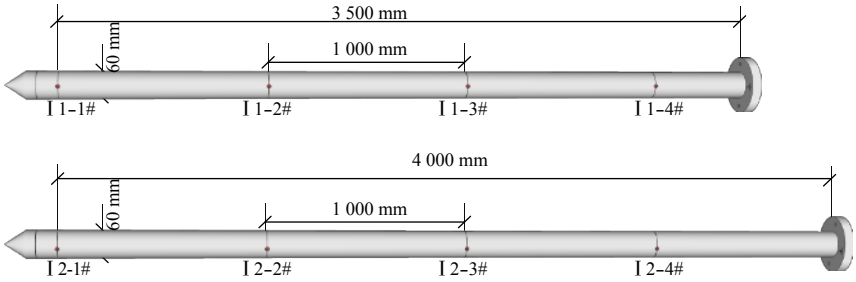

Fig. 3. The structure of pore pressure probe I 1 and I 2.

3.3 *Observation process*

During the second observation in December 2017, the automatic acquisition interval was 1 min and the continuous acquisition time was 3 600 s. Moreover, the acquisition frequency of 3 600 s was 1 Hz. The upper computer-controlled penetration device penetrated the 4.0 m pore pressure probe in 3 strokes, with a penetration depth of approximately 1.8 m, and each single stroke was approximately 30 s. The length of the equipment itself is approximately 0.5 m, and the depth of the buried hole is approximately 2.3 m. After a period of time, the stable observation data were obtained by the upper computer and the self-capacitance acquisition interval was changed to 20 min; the continuous acquisition time was 50 s, and the acquisition frequency within 50 s was 1 Hz. The observation time period was from December 25, 2017 to January 1, 2018.

4 Results and discussion

4.1 *Pore pressure distribution during penetration*

This observation shows that the depth of the pore pressure probe embedded in the sediment is approximately 2.3 m, with the relative position between the sensor and the seabed shown in Fig. 4. The pore pressure *in situ* observation lasted for 7 days, and more than 40 000 effective data points were obtained. The I 2–4# sensor had no signal return on site installation, though the remaining three sensors were in normal working condition. There was no extreme wind or wave action during the observation period. The probe penetrated during the day (December 25, 2017) because of field problems, and the probing was divided into two time periods, each with intervals of approximately 20 min; the *in situ* observations started after the target depth was reached. Through the mean filtering of raw data, the curves of pore pressure versus time were obtained, as shown in Fig. 5, and the eigenvalues of each sensor are shown in Table 1. The observation data can be divided into two stages, which are defined as “within 6 hours” and “after the end of 6 hours”.

For the I 2–1# sensor at the end of one hour (the occurrence of data singularity, as shown in Fig. 6), the measured pressure difference increased to 13.3 kPa. In addition, at the later stage of the *in situ* observation, the I 2–1# sensor measured the irregular fluctuation of pressure difference, and the maximum pressure fluctuation range reached 5 kPa. The I 2–1# sensor was unstable during the later observation.

4.2 *Pore pressure dissipation results*

The logarithmic curve of the pressure difference and time was measured by five sensors (Figs 7–9). For a period of time after the end of the penetration, the penetration of the excess pore pressure attenuated exponentially. Among the sensors, I 2–1#, I 2–2# and I 2–3# were affected by the penetration of the nearby probe during the observation period, leading to the sudden change in the observed data during the penetration of the excess pore pressure; as a result, the correlation between the pore pressure dissipation data after 50 min and the earlier data is poor. The specif-

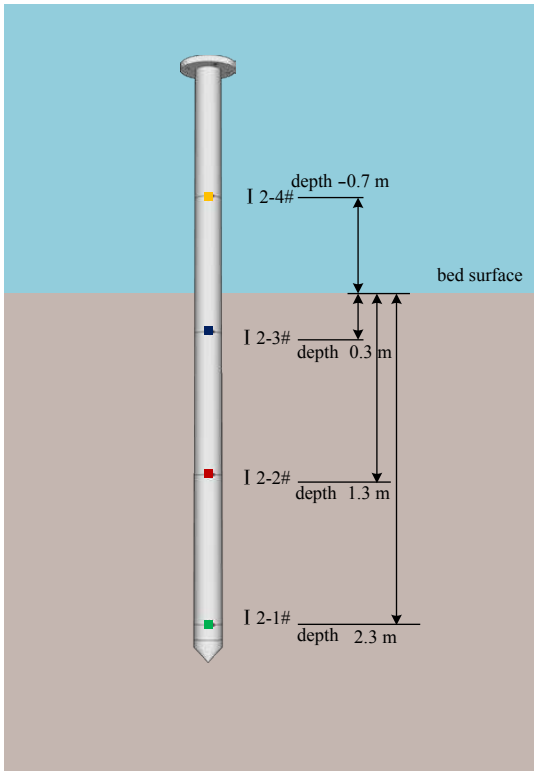

Fig. 4. The position of the transducer.

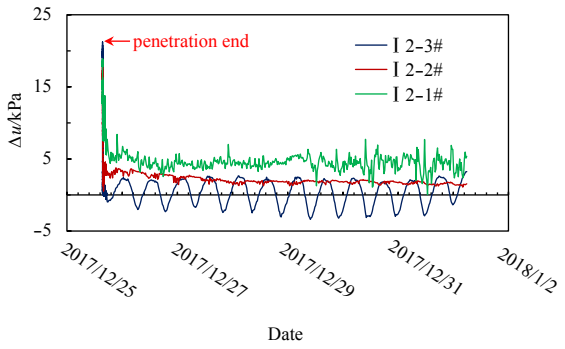

Fig. 5. Time history curve of measured differential pressure.

Table 1. Summary of measured differential pressure

Sensor number	Depth/m	Δu_{max}/kPa	Penetration end Δu_m/kPa	Δu_{min}/kPa
I 2–3#	0.3	21.2	21.2	–3.4
I 2–2#	1.3	18.2	18.2	0.6
I 2–1#	2.3	18.9	18.9	0.1

ic fitting formula and correlation coefficient are shown in Table 2.

According to the trend fitting formula of pressure $U(y)$ and time $t(x)$, the pressure difference rate recorded by the I 2–3# sensor was greater than that of the I 2–2# sensor, the former being approximately 2 times that of the latter. Additionally, the pressure difference dissipation rate recorded by the I 2–2# sensor was approximately 1.7 times that of the I 2–1# sensor. In addition, due to the effects of two penetration strokes, the I 2–1#, I 2–2#, and I 2–3# sensors recorded the pressure with a time dissipation curve, showing a brief rise in the pore pressure attenuation process after penetration.

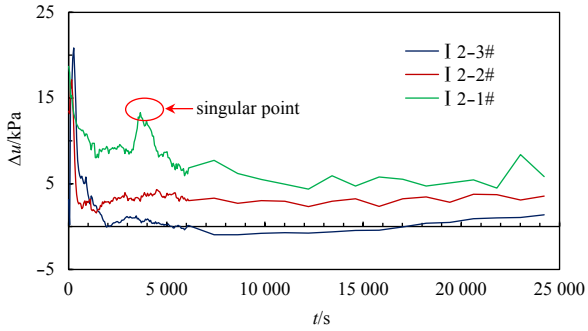

Fig. 6. Time history curve of I 2–1#, I 2–2# and I 2–3# measured differential pressure 6 hours after penetration.

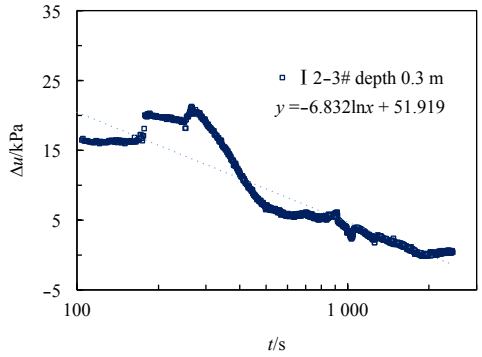

Fig. 7. Measurement of pressure difference and time logarithm curve of the I 2–3# transducer.

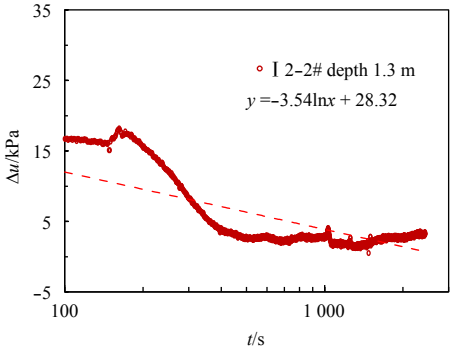

Fig. 8. Measurement of pressure difference and time logarithm curve of the I 2–2# transducer.

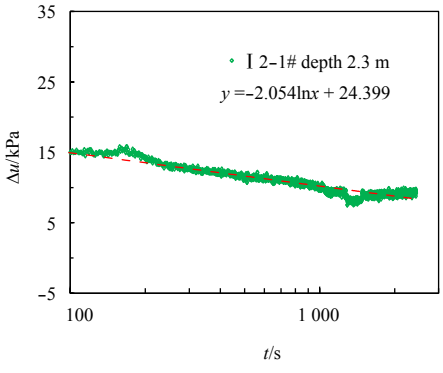

Fig. 9. Measurement of pressure difference and time logarithm curve of the I 2–1# transducer.

Table 2. Results of data fitting

Sensor number	Depth/m	Attenuation trend of hyperpore pressure with time	Correlation coefficient (R^2)	Slope	Intercept
I 2–3#	0.3	$y = -6.832\ln x + 51.919$	0.854 4	–6.832	51.919
I 2–2#	1.3	$y = -3.540\ln x + 28.320$	0.567 7	–3.540	28.320
I 2–1#	2.3	$y = -2.054\ln x + 24.399$	0.856 8	–2.054	24.399

On the basis of the Soderberg model, Bennet et al. (2002) proposed a formula for calculating the permeability index applicable to low-permeability clay:

$$k = \eta m_v \tau_{50} r_0^2 / t_{50}, \quad (2)$$

where t_{50} is the time required for the pore pressure to dissipate to 50% of the initial pore pressure, r_0 is the probe radius, and m_v is the volume compression coefficient.

Through the above Eq. (2), the *in situ* consolidation coefficient of the sediment can be easily calculated according to the *in situ* observation data, which is helpful for summarizing the relationship between penetration and pore pressure and the study of the *in situ* mechanical properties of the sediment.

The correlation curves of observation data of the I 2–1#, I 2–2# and I 2–3# sensors are poor. In this field of analysis, during this observation, two discontinuous penetration actions of the pore pressure observation rod occurred; that is, the second penetration action of the probe occurred 5 min after the first probe penetration was carried out. In the actual measurement process, the pore pressure dissipation of the sediment was measured in the sounding rod body of the I 2–2# and I 2–3# sensors. The value of the data is two times that of the disturbance. From the data curve, it can be seen that the apparent sudden pressure increase in the I 2–2#, I 2–3# and I 2–3# sensors corresponds to the two penetrations of the probe rod. Compared with the measurement data of the I 2–2# and I 2–3# sensors, the observation data of the I 2–1# sensor located at the tip of the cone is more stable, and as a result, the fitting degree of Eq. (2) is better.

The data of pore pressure dissipation recorded by the I 2–1#, I 2–2# and I 2–3# sensors were further analyzed and sorted, and the time required to remove the pore pressure recorded by each sensor to 50% was removed, with the specific data shown in Table 3. According to both the indoor test data obtained from the sampling points and the indoor laboratory tests, the G/Cu value of the test point is 100; therefore, the τ_{50} is 2.8, and the probe radius r_0 is 0.03 m. The above values can be input into Eq. (2) to calculate the horizontal consolidation coefficient of the sediment. The specific data are shown in Table 3.

According to the calculation results, the horizontal consolidation coefficient C_h is within the range of 1.3×10^{-6}–8.1×10^{-6} m^2/s, and the 0.5×10^{-6}–1.5×10^{-6} m^2/s obtained from the *in situ* indoor sampling consolidation test is within one order of magnitude.

Table 3. Summary of data

Sensor number	Depth below bed surface/m	t_{50}/s	Horizontal consolidation coefficient C_h/m^2·s^{-1}
I 2–4#	–0.7	–	–
I 2–3#	0.3	312	8.1×10^{-6}
I 2–2#	1.3	468	5.4×10^{-6}
I 2–1#	2.3	1 935	1.3×10^{-6}

In the application of the December 2017 observations, there was also a large difference in the time used by the sensors recorded at different depths to 50%. The t_{50} value recorded by the I 2–1# sensor of the cone tip of the probe is substantially greater than that of the I 2–3# and I 2–2# sensors located in the rod body, with the former approximately 3–6 times that of the latter. It is presumed that the sediment around the rod features not only as simple radial seepage diffusion of the rod body but also as diffusion along the rod body after the plastic failure of the sediment caused by the penetration of the rod so that the penetration of the penetration hole pressure of the rod body is faster than the penetration of the cone tip of the probe. Therefore, according to the I 2–3# and I 2–2# sensors of the probe rod body, the calculated value of the sediment horizontal directional consolidation coefficient is larger than that of the probe I 2–1# sensor.

Bennet's consolidation model does not fully consider the plastic deformation zone around the rod body and instead assumes that the horizontal consolidation coefficient C_h is constant throughout the process of penetration into the excess pore pressure. However, in practical observation, the calculation of pore pressure and pore pressure around the probe is more complex when the application of pore pressure observations is factored in, as the results assuming a constant value of C_h will overestimate the horizontal consolidation coefficient of the sediment.

4.3 *Pore pressure variation induced by tides*

To analyze the influence of tidal load on the pore pressure of sediment, the real-time water depth of the equipment was measured during the observation period. According to the local tide data, the real-time depth of water in December 2017 was calculated. The data of water depth during observation are shown in Table 4. The base water depth was completely stable at the completion time. The measured depth of water in December 2017 was 12 m. Figure 10 shows the changes in water depth related to penetration during observation.

It can be seen from the data curve that the periodic fluctuation of the data of the observed pore pressure in the observation from the I 2–3# and I 2–2# sensors in December 2017 was highly correlated with the tide change of the measured points after 6 hours of penetration. Figure 11 shows the comparison of the I 2–3# and I 2–2# sensors and the observed water depth change curve in December 2017.

The consistency of the three sensors was described according to the data curve. The variation of the excess pore water pressure exhibits hysteresis with respect to the water depth. The phase difference between these variables is approximately 1/4 T. In addition, the recorded tide caused by the pore pressure data with depth has a significant attenuation. Under the same tidal effect, the amplitude of pore water pressure observed by the I 2–3#

Table 4. Summary of water depth during observation

Maximum water depth h_{max}/m	Minimum water depthh_{min}/m	Base water depthh_0/m	Maximum tidal range		Minimum tidal range	
			Time	Δh_{max}/m	Time	Δh_{min}/m
13.76	10.18	12	15:00 Jan. 01, 2018	3.58	8:00 Dec. 26, 2017	1.59

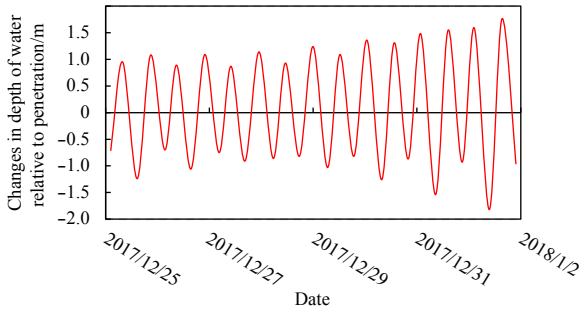

Fig. 10. Variation of water depth during observation.

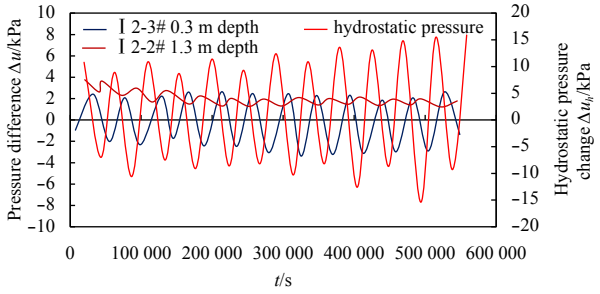

Fig. 11. Tidally induced pore pressure.

sensor can reach 4 kPa. The amplitude of excess pore water pressure observed by the I 2–2# sensor is below 2 kPa.

According to the observation data of the observation and application in December 2017, we can see that the I 2–2# sensor (buried depth 1.3 m) and the I 2–3# sensor (buried depth 0.3 m) both recorded the obvious change in tidal pore pressure.

The curves of peak and trough values recorded in the period of the I 2–2# and I 2–3# sensors are shown in Fig. 11. During the December 2017 test, the average period of water depth variation was 47 260 s, and the average periods of pressure fluctuation recorded by the I 2–2# and I 2–3# sensors were 52 405 s and 48 804 s, respectively. With the increase in burial depth, the variation in the pore pressure caused by tidal fluctuation was more obvious.

Hurley (1989) and Hurley and Schultheiss (1990) used the Biot consolidation theory to characterize the surface pressure in isotropic and porous elastic semi-infinite space and the difference in pore pressure, the pore pressure difference between the seabed surface and the sensors $|\Delta u|$ and its phase shift δ are obtained as follows:

$$|\Delta u| = (1-b)\, q_0 \left\{ \left[\mathrm{e}^{-\gamma z} \cos(-\gamma z) - 1 \right]^2 + \left[\mathrm{e}^{-\gamma z} \sin(-\gamma z) \right]^2 \right\}^{1/2}, \tag{3}$$

$$\delta = \tan^{-1} \left(\frac{\mathrm{e}^{-\gamma z} \sin(-\gamma z)}{\mathrm{e}^{-\gamma z} \cos(-\gamma z) - 1} \right), \tag{4}$$

where

$$b = \frac{(1+\phi)\, m_\mathrm{v} Q}{1 + (1+\phi)\, m_\mathrm{v} Q},$$

$$\gamma = \left(\frac{\omega \eta \left(1/Q + (1+\phi)\, m_\mathrm{v}\right)}{2k} \right)^{1/2},$$

$$Q = \left[\phi \beta_\mathrm{f} + (1-\phi)\, \beta_\mathrm{s} \right]^{-1},$$

and q_0 is the amplitude of the seafloor pressure variation, m_v is the volume compressibility, ϕ is porosity of the sediment, Q is Biot consolidation coefficient, and ω is the angular frequency, k is permeability coefficient of the sediment, β_f is volume compression coefficient of the Pore fluid, β_s is volume compression coefficient of the sediment.

Based on the *in situ* observation and indoor test data of the Ao Shan Wei, according to the above one-dimensional consolidation theory, the sediment is assumed to be isotropic, and the amplitude of the pore pressure fluctuation under the different permeation index is calculated with the depth. As shown in Fig. 12, the red circle and the blue box in the figure represent the I 2–2# and I 2–3# sensors, respectively, which measure the pressure difference. It can be seen that the pore pressure caused by permeability is smaller than that of sediment volume compression at 1.3 m below the seabed surface as measured by the I 2–2# sensor. According to the numerical calculation, the permeability index of the sediment is estimated to be between 1.0×10^{-17} m^2 and 1.0×10^{-18} m^2.

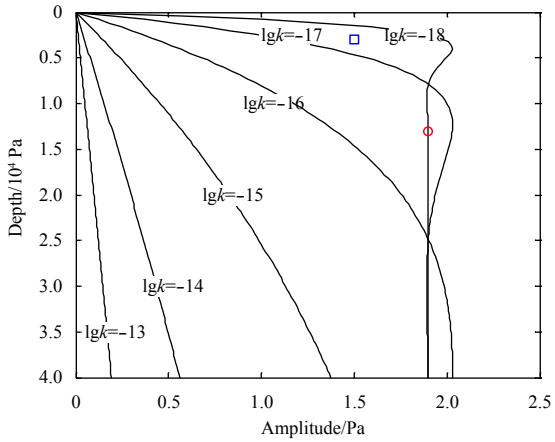

Fig. 12. Amplitude versus depth for different permeability. Red circle and blue box represent I 2–2# and I 2–3 sensors, respectively.

In addition, the results of numerical calculation show that when the permeability index k is below 1.0×10^{-18} m^2, the pore pressure rapidly decays at the depth of 0.5 m. According to this phenomenon, it is considered that the pore fluid permeation flow on the surface of the seabed has a low influence on pore pressure on the surface of the seabed, which is negligible; that is, the change in pore pressure in the sediments is caused by the volume compression of the sediments. Therefore, the diffusion component attenuates to 1. Equation (3) can be expressed in the following form:

$$|\Delta u_t| = q_0 (1-b) \cong q_0 \frac{\phi \beta_\mathrm{f}}{\phi \beta_\mathrm{f} + m_\mathrm{v}}. \tag{5}$$

Equation (5) ignores the compressive deformation of soil particles or sediment because β_s is much smaller than β_f. The volume compression coefficient m_v of the measured point is approximately 2.0×10^{-11} Pa^{-1}, and the 1.0×10^{-11}–1.0×10^{-10} Pa^{-1} obtained from the sample in the laboratory is within one order of magnitude.

5 Conclusions

(1) As a columnar rigid structure, the pore pressure probe can lead to the rapid accumulation of excess pore pressure in the sediments. In the *in situ* observations, the pressure difference recorded by the pore pressure probe can be divided into two stages: first, the stage in which the difference is caused by the penetration of hyperpore pressure and, second, the stage of environment-induced pore pressure fluctuation.

(2) In the silty sediment of the seabed, the penetration of the pore pressure attenuates exponentially, and the fluctuation of the pore pressure is consistent with the change in the environmental load; there is an obvious time lag and attenuation with depth.

(3) As there is a certain lag in the measurement of the maximum overpressure caused by the FBG pressure probe, the calculation of the consolidation coefficient of the sediment by the pore pressure dissipation model is not accurate. In general, the consolidation coefficient of the sediment will be overestimated.

(4) The pore pressure fluctuations caused by the tides can also be used to evaluate the parameters of the infiltration and consolidation of the sediments. Compared with the records of pore pressure dissipation caused by penetration, sediment permeability parameters calculated from the records of excess pore pressure fluctuation caused by tides or periodic loads are more accurate.

(5) The tidal pressure fluctuations in the low-permeability sediments rapidly decay to more than 10 meters below the seabed. The amplitude of tidal pressure fluctuation measured by the upper-end sensor of the probe is mainly controlled by the permeability index of the sediment, and that of the lower-end sensor of the probe is mainly controlled by the volume compression coefficient of the sediment.

References

Baligh M M. 1986. Undrained deep penetration, II: pore pressures. Géotechnique, 36(4): 487–501, doi: 10.1680/geot.1986.36.4.487

Bennett R H, Burns J T, Clarke T L, et al. 1982. Piezometer probes for assessing effective stress and stability in submarine sediments. In: Saxov S, Nieuwenhuis J K, eds. Marine Slides and Other Mass Movements. Boston, MA: Springer US, 129–161

Bennett R H, Faris J R. 1979. Ambient and dynamic pore pressures in fine-grained submarine sediments: Mississippi Delta. Applied Ocean Research, 1(3): 115–123, doi: 10.1016/0141-1187(79)90011-7

Bennett R H, Hulbert M H, Curry C, et al. 2002. *In situ* permeabilities of selected coastal marine sediments. IEEE Journal of Oceanic Engineering, 27(3): 571–580, doi: 10.1109/JOE.2002.1040939

Burns S E, Mayne P W. 1998. Monotonic and dilatory pore-pressure decay during piezocone tests in clay. Canadian Geotechnical Journal, 35(6): 1063–1073, doi: 10.1139/t98-062

Davis E E, Horel G C, MacDonald R D, et al. 1991. Pore pressures and permeabilities measured in marine sediments with a tethered probe. Journal of Geophysical Research: Solid Earth, 96(B4): 5975–5984, doi: 10.1029/91JB00220

Hurley M T. 1989. Application of Biot's theory to sea-bed sediments[dissertation]. Bangor: University of Wales

Hurley M T, Schultheiss P J. 1990. Sea-bed shear moduli from measurements of tidally induced pore pressures. In: Hovem J M, Richardson M D, Stoll R D, eds. Shear Waves in Marine Sediments. Dordrecht: Springer, 411–418

Lai J Y, Richards A F, Keller G H. 1968. In-place measurement of excess pore water pressure of gulf of main clays. San Francisco: American Geophysical Union Transactions

Li Bo. 2007. Study on cavity expansion and its applications to cone penetration test (in Chinese) [dissertation]. Dalian: Dalian University of Technology

Li Hongli. 2015. Application of Fiber Bragg Grating sensor in the monitoring of seabed excess pore water pressure (in Chinese) [dissertation]. Qingdao: Ocean University of China

Liu Tao, Cui Feng, Zhang Meixin. 2015. Research progress of deep seabed pore pressure observation techniques *in situ*. Journal of Hydraulic Engineering (in Chinese), 46(S1): 111–116

Liu Tao, Zhou Lei, Kou Hailei, et al. 2018. Model test of stratum failure and pore pressure variation induced by THF hydrate dissociation. Marine Georesources & Geotechnology, 1–8, doi: 10.1080/1064119X.2018.1458167

McPhail S D, Schultheiss P J. 1986. PUPPI-a free-fall seabed piezometer for geotechnical studies. In: Oceanology. Dordrecht: Springer, 249–258

Richards A F, Øten K, Keller G H, et al. 1975. Differential piezometer probe for an *in situ* measurement of sea-floor. Géotechnique, 25(2): 229–238, doi: 10.1680/geot.1975.25.2.229

Schultheiss P J. 1990. Pore pressures in marine sediments: An overview of measurement techniques and some geological and engineering applications. Marine Geophysical Researches, 12(1–2): 153–168, doi: 10.1007/BF00310570

Schultheiss P J, McPhail S D. 1986. Direct indication of pore-water advection from pore pressure measurements in Madeira Abyssal Plain sediments. Nature, 320(6060): 348–350, doi: 10.1038/320348a0

Sills G C, Nageswaran S. 1984. Compressibility of gassy soil. In: Spearhead Exhibitions, Ltd, ed. Oceanology International. Brighton: Society for Underwater Technology, 1–26

Sultan N, Bohrmann G, Ruffine L, et al. 2014. Pockmark formation and evolution in deep water Nigeria: Rapid hydrate growth versus slow hydrate dissolution. Journal of Geophysical Research: Solid Earth, 119(4): 2679–2694, doi: 10.1002/2013JB010546

Sultan N, Cattaneo A, Sibuet J C, et al. 2009. Deep sea *in situ* excess pore pressure and sediment deformation off NW Sumatra and its relation with the December 26, 2004 Great Sumatra-Andaman Earthquake. International Journal of Earth Sciences, 98(4): 823–837, doi: 10.1007/s00531-008-0334-z

Sultan N, Lafuerza S. 2013. *In situ* equilibrium pore-water pressures derived from partial piezoprobe dissipation tests in marine sediments. Canadian Geotechnical Journal, 50(12): 1294–1305, doi: 10.1139/cgj-2013-0062

Sultan N, Voisset M, Marsset B, et al. 2007. Potential role of compressional structures in generating submarine slope failures in the Niger Delta. Marine Geology, 2007, 237(3–4): 169–190

Terzaghi K. 1943. Theoretical Soil Mechanics. New York: John Wiley and Sons, 25–32

Urgeles R, Canals M, Roberts J, et al. 2000. Fluid flow from pore pressure measurements off La Palma, Canary Islands. Journal of Volcanology and Geothermal Research, 2000, 101(3–4): 253–271

Vanneste M, Sultan N, Garziglia S, et al. 2014. Seafloor instabilities and sediment deformation processes: The need for integrated, multi-disciplinary investigations. Marine Geology, 352: 183–214, doi: 10.1016/j.margeo.2014.01.005

Ye Yincan. 2011. Review of the development of marine hazard geology and its future prospects. Journal of Marine Sciences (in Chinese), 29(4): 1–7